J Sol-Gel Sci Technol (2018) 85:66–75
DOI 10.1007/s10971-017-4512-y

ORIGINAL PAPER: NANO-STRUCTURED MATERIALS (PARTICLES, FIBERS, COLLOIDS, COMPOSITES, ETC.)

Synthesis of ZnO nanoparticles and a composite with polyacrylamide in acrylamide solutions

Vladimir Tatarchuk[1] · **Irina Druzhinina**[1] · **Vladimir Zaikovskii**[2] · **Evgeny Maksimovskii**[1] · **Ilia Korolkov**[1] · **Olga Antonova**[1]

Received: 12 July 2017 / Accepted: 14 September 2017 / Published online: 17 October 2017

Abstract The use of solutions of acrylamide (AAm) opens up new ways for easy one-step synthesis of ZnO nanoparticles (NPs) and their composites with polyacrylamide (PAAm). To obtain a nanocrystalline product in which the composition of NPs is close to $\{(ZnO)_m(Zn^{2+})_n\}(CH_3COO^-)_{2n}$ with $n/m = 0.292$, the hydrolysis of Zn $(CH_3COO)_2{\cdot}2H_2O$ should be carried out in 96% ethanol. In this process, AAm plays the role of an organic base that accepts protons and does not act as a protective ligand. The ZnO NPs/PAAm composite is formed as a viscous transparent colorless hydrogel if the same reaction is carried out in an aqueous medium simultaneously with the radical polymerization of AAm initiated by $(NH_4)_2S_2O_8$. A solid composite can be isolated due to the destruction of the hydrogel by the addition of ethanol. In the composite, PAAm acts as a polymeric matrix in which ZnO NPs are distributed. The synthesis products were characterized by XRD, TEM, SEM, EDX, DLS, IR, Raman scattering, photoluminescence, and chemical analysis. The particles in both products were nanocrystals of hexagonal ZnO about a few nanometers in size. The powder of $\{(ZnO)_m(Zn^{2+})_n\}(CH_3COO^-)_{2n}$ NPs had a yellow photoluminescence with emission maximum at $\lambda_{em} = 590$ nm. The photoluminescence band of the ZnO NPs/PAAm hydrogel had a maximum at $\lambda_{em} = 449$ nm.

Graphical abstract

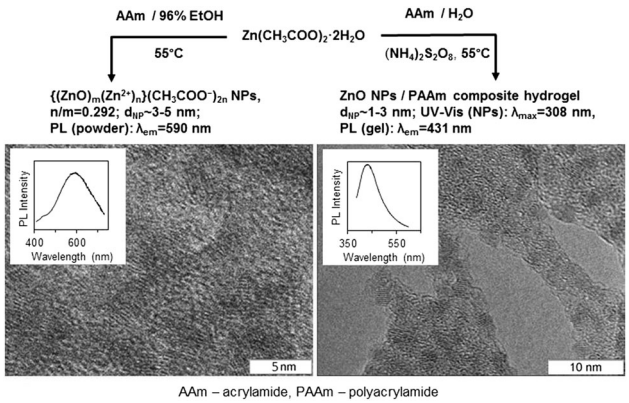

AAm – acrylamide, PAAm – polyacrylamide

Keywords Nanoparticles · Nanocomposite · Zinc oxide · Acrylamide · Polyacrylamide · Synthesis

1 Introduction

Zinc oxide nanoparticles (NPs) possess a broad range of useful properties (semiconducting, magnetic, optical, luminescence, chemical), are non-toxic and relatively stable chemically and thermally. Due to these properties, they play essential part in the development of new materials for electronics and optoelectronics [1–4], photovoltaics [5–7],

Electronic supplementary material The online version of this article (https://doi.org/10.1007/s10971-017-4512-y) contains supplementary material, which is available to authorized users.

✉ Vladimir Tatarchuk
tat@niic.nsc.ru

[1] Nikolaev Institute of Inorganic Chemistry, Siberian Branch, Russian Academy of Sciences, Ac. Lavrentyev pr., 3, Novosibirsk 630090, Russia

[2] Boreskov Institute of Catalysis, Siberian Branch, Russian Academy of Sciences, Ac. Lavrentyev pr., 5, Novosibirsk 630090, Russia

photocatalysis [8], chemical sensing [9, 10], biomedical visualization and marking [11, 12], as well as in the development of the preparations with antiseptic, bactericidal, and cytotoxic action in medical nanotechnologies [13–15].

A large number of methods to obtain ZnO NPs are known, including chemical methods working in solutions [8, 16]. Among them are widespread syntheses, which include the hydrolysis of Zn^{2+} salts in an alcohol-containing medium based on ethanol (EtOH) [12,17–20], isopropanol (*i*-PrOH) [21–23], methanol (MeOH) [17, 24], benzyl alcohol (BnOH) [25], 2-methoxyethanol (2-ME) [17]. In many cases, hydrolysis is carried out in the presence of strong bases (LiOH, NaOH, KOH, $(CH_3)_4NOH$), however, additional purification of ZnO from the compounds containing alkaline metal cations is necessary. To stabilize the NPs, provide a narrow size distribution or render definite physicochemical properties to the surface of NPs, functionalized organic compounds are introduced into the reaction mixture during the synthesis. These compounds act as protective ligands, for example octanethiol, dodecanethiol, octanedodecylsulfonic acid, dopamine (Electronic Supplementary Material, Table S1).

In this paper, we investigated solutions of acrylamide (AAm) in 96% ethanol and water as new reaction media for the synthesis of ZnO nanoparticles and a "NPs/polymer" type composite in the form of a hydrogel. AAm molecules have vinyl, carbonyl, and amide functional fragments. Due to the electron-donor properties of the amide group, AAm can play the role of a protective ligand, as is observed for Au NPs [26], or act as an organic base that accepts protons arising during the reactions. Due to the vinyl group, AAm can polymerize into polyacrylamide (PAAm) [27], used to produce micro-patterned gel structures for many applications, particularly in biotechnology area [28]. Taking into account solubility in ethanol-AAm is soluble, PAAm is insoluble (both compounds are soluble in water)-syntheses of NPs and composite gel by hydrolysis of zinc acetate were carried out in 96% ethanol and water, respectively. To synthesize the composite gel, the hydrolysis of zinc acetate was carried out simultaneously with the radical polymerization of AAm initiated by $(NH_4)_2S_2O_8$. We expected that AAm, which is taken for synthesis in excess, will promote the hydrolysis of the zinc salt by binding the emerging protons: $Zn^{2+} + H_2O + 2\,CH_2CHC(O)NH_2 \rightarrow ZnO + 2\quad CH_2CHC(O)NH_3^+$. The amide groups of polyacrylamide should also have similar basic properties.

Data are available on acrylamide products with micro-sized ZnO particles, which improve the physico-chemical characteristics of the drilling fluid for effective oil extraction [29]; no other data on the ZnO NPs associated with AAm or PAAm was found.

2 Experimental

2.1 Materials

Zinc acetate dihydrate (Kh. Ch.–chemically pure grade, Chimmed, Russia), acrylamide for electrophoresis (>99.0%, Os. Ch.–specially pure grade, Medigen, Russia), ammonium persulfate (reagent grade, 98%, Sigma-Aldrich), and rectified 96% ethanol were used without further purification.

2.2 Synthesis of ZnO NPs in ethanol

A mixture of solid substances: 0.232 g Zn $(CH_3COO)_2{\cdot}2H_2O$ (1.1 mmol) and 0.180 g AAm (2.5 mmol) was placed in a broad vial; 25 ml of 96% ethanol was added, and mixing was carried out. The resulting turbid solution was homogenized for 5 min with ultrasound, then heated for 4 h inside a drying chamber at 55 °C in the closed vial. After cooling to room temperature, a transparent colorless solution and voluminous white precipitate were obtained. The vial with solution and precipitate was sonicated for 5 min. About 1 ml of suspension was taken from the vial for TEM examination (sample **I**). After suspension settling, again a transparent solution (colloid, judging from its ability to scatter laser beam) and a voluminous white precipitate were obtained. About 1 ml of the transparent supernatant was taken for TEM (sample **II**). The precipitate was centrifuged, separated from the liquid phase, washed with ethanol, and dried at a temperature of 130 °C (sample **I-130**) then a part of the substance was additionally heated at 300 °C for 1 h (sample **I-300**). The samples were stored in a desiccator above P_2O_5.

In connection with the synthesis in alcoholic media, we noted one interesting experimental fact, although not directly related to this work. In one of the preliminary experiments on the synthesis of ZnO NPs by the reaction of zinc acetate with KOH, the solvent was not ethanol but isopropanol which was stored for a long time in the laboratory, and which evidently had accumulated a significant amount of peroxide compounds due to oxidation in the air. As a result, the product of synthesis turned out to be the NPs of ZnO_2 about 4–5 nm in size. The experiment was repeated, and the result was reproduced in full.

2.3 Synthesis of ZnO NPs/PAAm composite in water

Twenty five milliliter of water was added to a mixture of 0.221 g of $Zn(CH_3COO)_2{\cdot}2H_2O$ (1.0 mmol) and 1.25 g of AAm (18 mmol) in a broad vial. The sonication was carried out for 5 min. A transparent solution was obtained. Then ~6 mg of $(NH_4)_2S_2O_8$ (0.03 mmol) was added as an initiator of the radical polymerization of AAm [27, 28]. Heating for

4 h inside the drying chamber at 55 °C in the closed vial was carried out. A transparent colorless product in the form of hydrogel was obtained. It was scattering the laser beam and characterized by high viscosity. About 1 ml of the product was sampled for TEM (sample **III**), a fraction was left for the examination by dynamic light scattering (DLS), while the rest fraction was transferred into a separate test tube, and ethanol was added at a volume ratio of 1:1. Flaky white precipitate was immediately formed. The mixture in the test tube was sonicated; about 1 ml of the resulting suspension was taken for TEM (sample **IV**). The composite hydrogel synthesized in this way was stable: its appearance did not change during observations for 9 months. The synthesis of PAAm hydrogel was carried out in parallel with the synthesis of the composite under the same conditions but without $Zn(CH_3COO)_2{\cdot}2H_2O$.

3 Methods

The average hydrodynamic diameter of the particles in hydrogel **III** was measured by DLS at an angle of 90° in a quartz cell with a cross section of 1 cm^2 at room temperature with the help of a 90Plus spectrometer (Brookhaven Inst). To remove dust, liquid samples were many times passed through a FPV-403-030 membrane (Jet Biofil) with pore diameter 0.45 μm.

XRD examination of NPs samples **I-130** and **I-300** was carried out with a Shimadzu XRD-7000 diffractometer (CuKα radiation, Ni filter, Bragg–Brentano arrangement, scintillation detector, room temperature) within the angle range 2θ from 5° to 60°. Scanning step was 0.03°, the time of accumulation in a point was 1 s. The samples for measurements were prepared by drying the suspension in heptane at the polished side of the quartz cell at room temperature. Indexing of diffraction patterns was carried out relying on the PDF database, release 2010. Crystallite size was calculated using the Scherrer equation and three individual peaks of ZnO at 31.8° (100), 36.3° (101), and 56.6° 2θ (110) taking into account the half-width of the peaks of reference Si.

The morphology, size and composition of the particles in the suspension in ethanol (sample **I**) and in supernatant (sample **II**), as well as in hydrogel (sample **III**) and precipitated composite (sample **IV**) were studied by means of TEM, HRTEM, and SAED with a JEM-2010 instrument (JEOL Ltd.) with the accelerating voltage of 200 kV. For measurement, a drop of the dispersion of NPs sample treated with ultrasound was dried on a thin perforated carbon film substrate fixed on a copper grid.

Examination of NPs by means of SEM and EDX was carried out with a JSM-6700F instrument (JEOL) equipped with an energy-dispersive X-ray analyzer EX-23000BU. Accelerating voltage was 5 keV, the working distance was 3 mm, the detector of secondary electrons was used to record the images. The samples were prepared by evaporating the drops of ethanol suspensions of NPs precipitate dried at 130 °C (sample **I-130**) and heated at 380 °C (sample **I-380**). Evaporation was performed on silicon substrates. Then a conducting layer of Au-Pd alloy was deposited on the samples.

The Raman spectra of the NPs powder dried at 130 °C (sample **I-130**) were recorded with a LabRAM HR spectrometer (Horiba) in the back-scattering geometry using the 633 nm line of a He–Ne laser and a Raman microscope. The spectral resolution was 2.5 cm^{-1}.

The IR spectra of powder samples prepared by pressing as tablets with KBr were recorded with Scimitar FTS 2000 instrument within the range 375–4000 cm^{-1} and Vertex 80 within the range 100–600 cm^{-1}.

The spectra of photoluminescence (PL) and excitation of luminescence (EL) for powders of NPs (sample **I-130**) and AAм, as well as for the hydrogels of ZnO NPs/PAAm (sample **III**) and PAAm were recorded with a Fluorolog-3 spectrofluorimeter (Horiba Jobin Yvon) with a cooled module of photon registration PC177CE-010 equipped with a photo-electronic multiplier R2658.

Analyses of the NPs sample **I-130** on Zn content (atomic absorption after the acid dissolution of the sample) and C, H, N (microanalysis) were carried out at the Analytical Laboratory of Nikolaev Institute of Inorganic Chemistry.

4 Results and discussion

4.1 Characterization of ZnO NPs from ethanol

As stated above, the synthesis products in the ethanol solution of AAm were a voluminous white precipitate suspended in the lower layer of the liquid phase and a transparent, colorless solution in the upper layer that scattered the laser beam, therefore it contained colloidal particles.

The TEM data for the samples of products prepared as films on substrates by the evaporation of suspension drops (sample **I**) or supernatant (sample **II**) containing excess solid AAm along with NPs are shown in Fig. 1. As expected, the particles in the sedimentation precipitate were somewhat larger than the particles that were not settled from the supernatant and had a size of about 3–5 nm. Judging from the SAED electron diffraction patterns, both samples of NPs were polycrystalline and related to the hexagonal phase of ZnO. The SAED pattern of sample **I** (Fig. 1a, inset) showed the hexagonal arrangement of arched reflections with substantial azimuthal broadening $\pm\Delta \approx 20$ degrees. The circular kind of diffraction (without arched

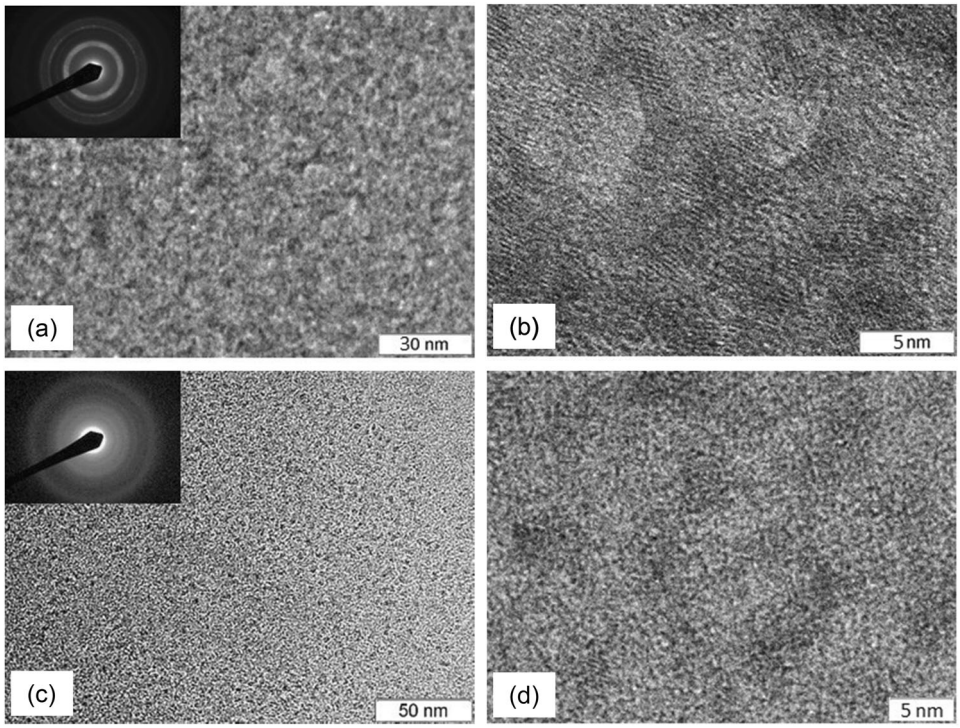

Fig. 1 **a** TEM and **b** HRTEM images of ZnO NPs of sample **I**; **c** TEM and **d** HRTEM images of ZnO NPs of sample **II**; the insets show the SAED data

reflections) for sample **II** (Fig. 1c, inset) is the evidence of the stronger disordering of NPs after their aggregation in the form of a film. At the same time, for NPs 3–5 nm in size, HRTEM images (Fig. 1d) reveal periodicity characteristic of interplanar spacings $d_{100} = 0.28$ nm of the nanocrystalline ZnO phase [30].

The results of XRD studies for the NPs precipitate, isolated, washed and dried at 130 °C (sample **I-130**) and 300 °C (sample **I-300**), confirmed that the product contained one crystal phase of ZnO (Fig. 2). Crystallite sizes estimated on the basis of XRD data were somewhat different for different 2θ and increased with an increase in temperature (Table 1). These estimations gave large NP size than the size of NPs observed in TEM images shown in Fig. 1, thus, isolation from solution and drying of NPs precipitate was accompanied by a slight increase in the linear dimensions of NPs in different directions.

SEM images of the samples **I-130** and **I-300** showed that they were composed of oblong aggregates of NPs, with cross section of the order of 10^1 nm and the length ~10^2 nm. The appearance of the aggregates did not change after drying temperature was increased from 130 to 300 °C (Fig. 3). The EDX spectrum of the sample **I-130** deposited on a silicon substrate contained intense lines of Zn and O from particles, the line of Si from the substrate, and a low-intensity line of C that could be attributed to AAm and the products of its reactions or to the initially introduced CH_3COO^- ions. Besides, lines of nitrogen were not

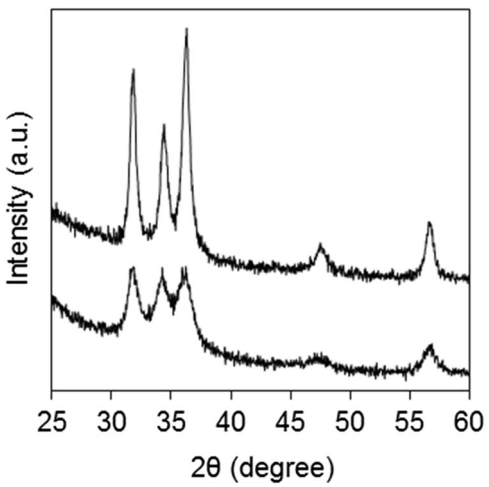

Fig. 2 XRD patterns of samples **I-130** (lower line) and **I-300** (upper line)

observed in an explicit form. A similar situation was for sample **I-300**.

Raman and IR spectra of sample **I-130** shown in Fig. 4 differed from the known spectra of AAm and PAAm, in particular, the bands of vibrations related to the amido group were absent [31, 32]. At the same time, they were concordant with the combinations of the known spectra of ZnO [33, 34] and CH_3COO^- in the salts with Zn^{2+}, Pb^{2+}, Li^+ [35]. This was also evidenced by the experimental

spectra of reference substances, that were reagents such as ZnO powder for phosphors and crystalline salt of chemically pure $Zn(CH_3COO)_2{\cdot}2H_2O$. In the Raman spectra of sample **I-130**, the peaks at 98, 336, and 436 cm^{-1} are related to ZnO, while the peak at 220 cm^{-1} and all the peaks within the range 600–3200 cm^{-1} are related to CH_3COO^- (Table 2). Similarly, comparing the IR spectra with the spectra of reference substances, we state that absorption related to ZnO was observed in the IR spectrum of sample **I-130** within the range 300–600 cm^{-1}, while the bands in the region 600–3600 cm^{-1} were due to the vibrations in CH_3COO^- (Fig. 4b, Table S2).

4.2 Chemical composition of ZnO NPs

The chemical analysis confirmed the absence of nitrogen in sample **I-130**, therefore AAm was absent. The detected Zn, C, and H content was in good agreement with the calculated content of these elements in the particle having conditional composition $\{ZnO\}_m\{Zn(CH_3COO)_2\}_n$ or $ZnO_{1/(1+n/m)}(CH_3COO)_{2(n/m)/(1+n/m)}$ calculated per one Zn atom for the ratio of $n/m = 0.292$, which was optimized by the least squares method (Table 3). Agreement was also observed for the formula mass M* and for the H/C atomic ratio.

Table 1 Crystallite sizes, evaluated from XRD data

Samples	Sizes (nm) for 2θ angles:		
	31.8°	36.3°	56.6°
I-130	14.5 ± 1.5	15.2 ± 1.5	8.9 ± 0.9
I-300	19.0 ± 2.0	14.7 ± 1.5	18.0 ± 1.8

According to the notion about the structure of NPs, Zn^{2+}, and CH_3COO^- ions should most probably belong to the surface layer. The adsorption of CH_3COO^- ions on the ZnO NPs surface has already been reported [23]. Therefore, the particles can be represented as $\{(ZnO)_m(Zn^{2+})_n\}(CH_3COO^-)_{2n}$, where n surface cations Zn^{2+} make the charge of the particle which is compensated by 2n anions CH_3COO^-. From the viewpoint of composition, this stoichiometry is formally equivalent to the above-indicated stoichiometry $\{ZnO\}_m\{Zn(CH_3COO)_2\}_n$. As for AAm, it probably has an insufficient affinity for ZnO to play the role of a protective ligand, as was the case with Au NP [26]. Thus, in the synthesis of NPs in ethanol, AAm acts only as organic base which binds H^+ ions formed during the hydrolysis of $Zn(CH_3COO)_2{\cdot}2H_2O$.

4.3 Modeling of ZnO NPs by "equivalent spheres" method

The absolute values of m and n were estimated using the equivalent spheres approach on the basis of experimentally determined stoichiometric ratio $n/m = 0.292$. Within this

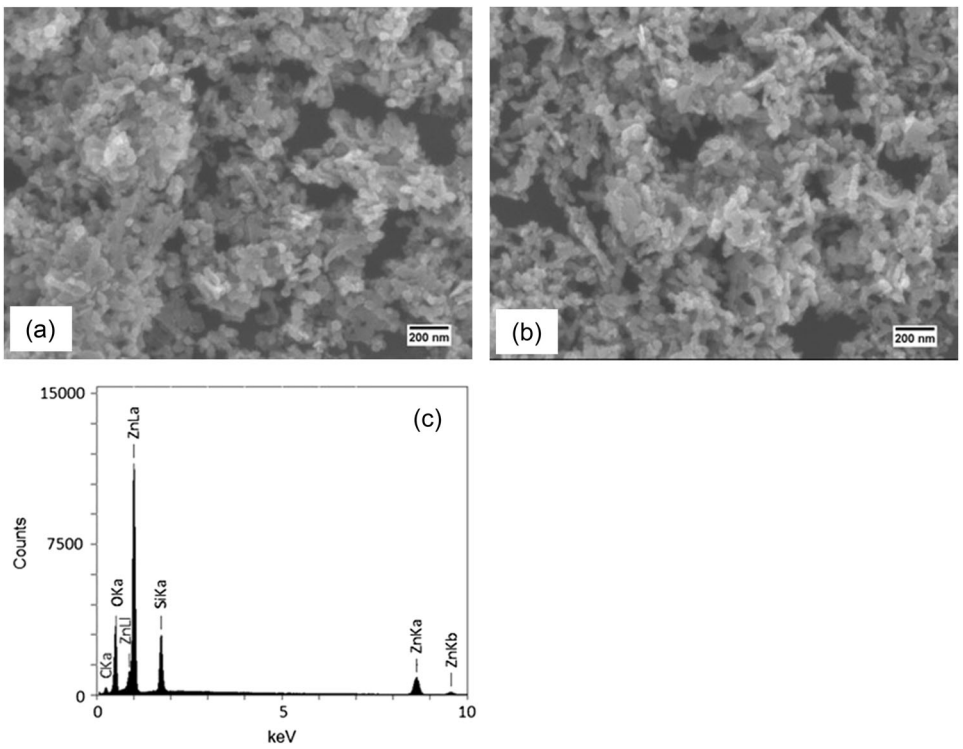

Fig. 3 SEM images of samples **a I-130** and **b I-380**; **c** EDX analysis of sample **I-130**

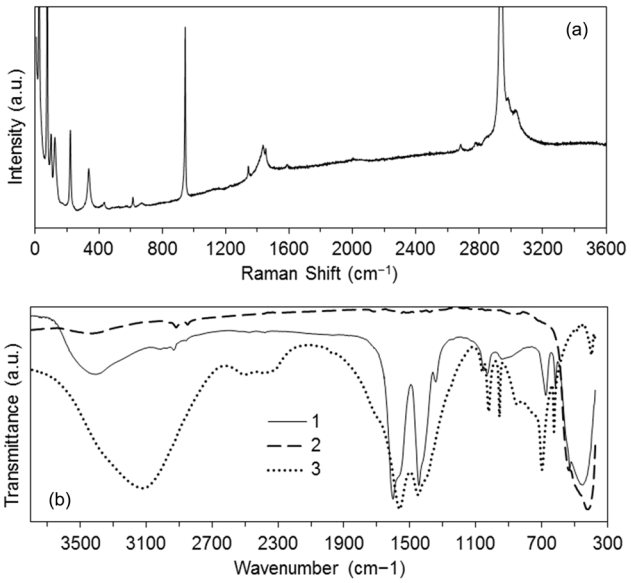

Fig. 4 **a** Raman spectrum of sample **I-130**; **b** IR spectra of sample **I-130** (1) and reference substances ZnO (2) and $Zn(CH_3COO)_2{\cdot}2H_2O$ (3)

approach, the molecules of a crystalline substance are represented as spheres with the volume V which is equivalent to the V_{cell}/z ratio, where V_{cell} and z are the unit cell volume of the crystal and the number of formula units per cell. Taking into account available crystallographic data [30, 36, 37] the equivalent volumes of molecules and the corresponding radii were estimated as $V_1 = 0.02388\ nm^3$, $r_1 = 0.179$ nm for ZnO and $V_2 = 0.1656\ nm^3$, $r_2 = 0.341$ nm for $Zn(CH_3COO)_2$. Similar values were also obtained in the calculations of these parameters from the known densities of ZnO (5.61 g/cm^3) and $Zn(CH_3COO)_2$ (1.84 g/cm^3). The problem of the estimation of m and n values was formally reduced to the determination of radius R for a sphere with volume V_c inside which it would be possible to accommodate m balls with radius r_1, and on its surface it would be possible to place n balls with radius r_2 in the form of a monolayer (Scheme S1). The relationships of R with the volume parameters of the nanoparticle is shown by the equations: $V_{NP} = (4/3)\pi(R + 2r_2)^3$–volume of the $\{ZnO\}_m\{Zn(CH_3COO)_2\}_n$ particle, $V_c = (4/3)\pi R^3$–volume of the $\{ZnO\}_m$ spherical fragment, $V_s = V_{NP} - V_c = (4/3)\pi\{(R + 2r_2)^3 - R^3\}$–volume of the $\{Zn(CH_3COO)_2\}_n$ surface layer. Then, $m = V_c/V_1$, $n = V_s/V_2$ and $n/m = \{(1 + 2r_2/R)^3 - 1\}(V_1/V_2)$. For $n/m = 0.292$, we obtained $R \approx 1.53$ nm, as well as $V_c \approx 14.9\ nm^3$, $m \approx 624$, $V_s \approx 30.2\ nm^3$, $n \approx 182$. The volume of the last spherical layer of ZnO molecules in direct contact with the outer layer of $Zn(CH_3COO)_2$ molecules was $V_l = (4/3)\pi\{R^3 - (R - 2r_1)^3\} \approx 8.2\ nm^3$ and contained $m_l = V_l/V_1 \approx 344$ molecules. Therefore, the actual ratio was $n/m_l \approx 0.53$, that is, there was about 1 $Zn(CH_3COO)_2$ molecule per two ZnO molecules on the surface of NP.

Table 2 Wavenumbers (cm^{-1}) of peaks in the Raman spectrum of sample **I-130** of ZnO NPs and the known data for ZnO [33], [34] and CH_3COO^- in $Zn(CH_3COO)_2{\cdot}2H_2O$ [35] and $Pb(CH_3COO)_2{\cdot}3H_2O$ [35]

I-130	ZnO		CH_3COO^-	
	(a)	(b)	(c)	(d)
74				
98	98			
123				
220			231, 257	
336	331	330		
436	438	437		
614			~620	617
671			696	671
945			956	935, 955
1343			~1350	1354
1435				1428
1452			~1450	1459
2937			2939	2931
2982				2983
3027				3008

Table 3 Characteristics of the NPs composition, determined in the analysis of sample **I-130** and calculated for $ZnO_{1/(1+n/m)}(CH_3COO)_{2(n/m)/(1+n/m)}$ at $n/m = 0.292$

	Composition (wt.%)				H/C (mol/mol)	M* (g/mol)
	Zn	C	H	N		
Determined	62.0	10.3	1.30	<0.05	1.51	105.4
Calculated	62.6	10.4	1.30	–	1.50	104.4

Note: H/C is the atomic ratio of hydrogen to carbon

M* is the formula mass

This result correlates with the fact that the equivalent spherical radius of ZnO molecule is about twice smaller than the corresponding value for $Zn(CH_3COO)_2$–$r_1/r_2 \approx 0.52$. The size of the equivalent spherical particle was estimated as $d_{NP}^* = 2(R + 2r_2) \approx 4.4$ nm, which agreed with TEM results.

It is interesting to note that a $[Zn_4O(CH_3COO)_6]$ cluster was reported [38], which can be formally represented as $\{ZnO\}\{Zn(CH_3COO)_2\}_3$ and considered as a minor term of the same series of particles as those obtained by us $\{ZnO\}_m\{Zn(CH_3COO)_2\}_n$, but with $m = 1$ and $n = 3$.

4.4 PL data for ZnO NPs powder

The normalized EL and PL spectra of the NPs powder (sample **I-130**) are shown in Fig. 5. In the PL spectrum,

under excitation at $\lambda_{ex} = 340$ nm, two bands with emission maxima at $\lambda_{em} = 384$ and 577 nm were observed. Under excitation at $\lambda_{ex} = 390$ nm, the PL spectrum was a single broad band with the maximum at $\lambda_{em} = 590$ nm. As it is known, the PL band in the UV region is caused by the recombination of free excitons, and the yellow emission in the visible region is associated with oxygen vacancies in the structure of ZnO NPs [39–41].

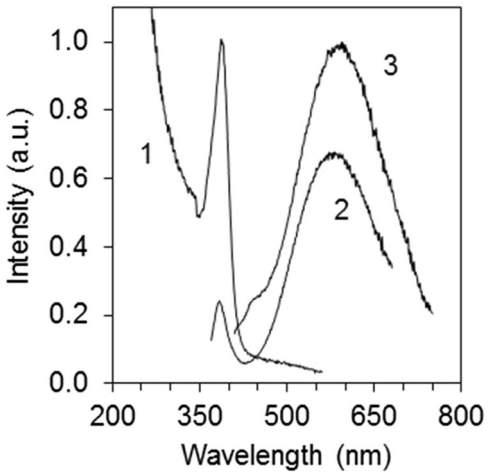

Fig. 5 Normalized luminescence spectra of ZnO NPs in the powdered sample **I-130**: EL at $\lambda_{em} = 590$ nm (1), PL at $\lambda_{ex} = 340$ nm (2) and PL at $\lambda_{ex} = 390$ nm (3)

4.5 Characterization of ZnO NPs/PAAm composite from water

Though AAm turned out to be useless as a protective ligand, $Zn(CH_3COO)_2$ hydrolysis and AAm polymerization proceeding concurrently in the aqueous medium resulted in obtaining a composite material which was ZnO NPs distributed in the PAAm matrix. The synthesis product looked like a viscous transparent colorless hydrogel.

An attempt to estimate the size of polymer particles by means of DLS directly in the hydrogel (sample **III**) showed unreliability in the measurement data because of the polymodal distribution and a large value of the average hydrodynamic diameter at a level of 10^4–10^5 nm. After 1000-fold dilution with deionized water and multiple filtration through a membrane with pore size 0.45 μm, monomodal distribution was obtained, with the average hydrodynamic diameter of PAAm particles and standard deviation for 60 measurements equal to 448 ± 62 nm. Thus, the basis of the gel were polymer particles of PAAm, ≥400 nm in size.

TEM images of sample **III** clearly exhibit a polymeric matrix with ingrained NPs crystals (Fig. 6a,b). The crystallite sizes in different projections were estimated at 1–3 nm. The SAED image in the inset in Fig. 6a contains diffusely broadened circular reflections 100, 002, 101, 110, 103 etc., which points to the chaotic orientation of NPs crystallites in the polymeric matrix. Several nanocrystals about 2 nm in size with the most pronounced structure are

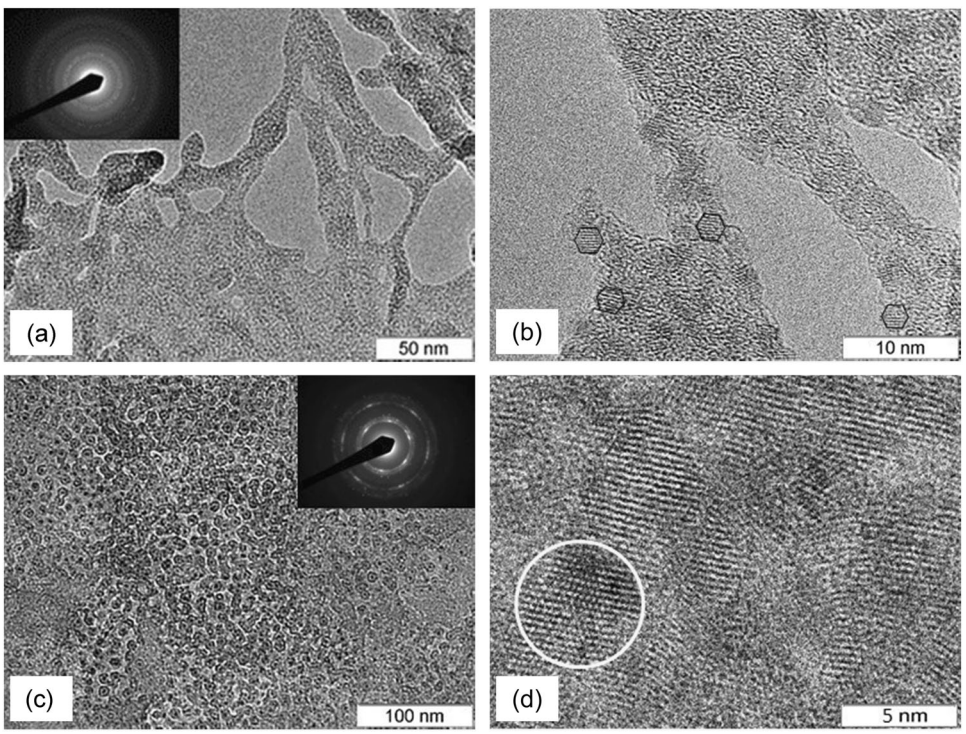

Fig. 6 **a** TEM and **b** HRTEM images of ZnO NPs in sample **III**, several nanocrystals with the most pronounced structure are marked by hexagonal frames corresponding to their shapes; **c** TEM and **d** HRTEM images of ZnO NPs in sample **IV**, one of the ZnO nanocrystallites is marked with a white circle; the insets show the SAED data

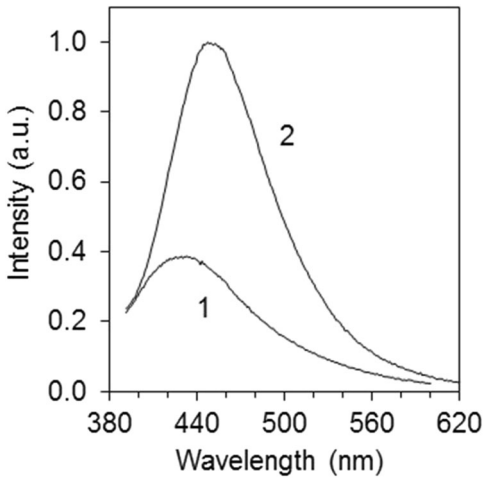

Fig. 7 Normalized PL spectra of hydrogels of the ZnO NPs/PAAm composite (1) and PAAm (2), $\lambda_{ex} = 330$ nm

marked in Fig. 6b by hexagonal frames corresponding to their shapes.

To precipitate the solid ZnO NPs/PAAm composite, the hydrogel was destroyed by adding ethanol in which PAAm is insoluble. The deposited composite (sample **IV**) contained NPs in more concentrated form, which was evidenced by the dense arrangement of NPs on the substrate, observed in TEM images and confluence of the structural pictures from separate particles in HRTEM images (Figs. 6c, d). It should be noted that NPs appeared in the TEM images of sample **IV** (Fig. 6c) gradually during the destruction of the polymeric matrix under the action of the electron beam. The size of ZnO crystallites was about 5 nm. The SAED picture presented in the inset in Fig. 6c points to the formation of the crystallographic texture with the axis of the zone [001] for diffraction reflections. In this situation, reflections 100 and 110, belonging to this zone, have the azimuthal broadening $\pm\Delta \approx 5$ degrees. Thus, it may be concluded that the crystallites, initially disoriented chaotically, then with an increase in their size to 5 nm form a better oriented ZnO particles layer with the *C* axis going perpendicularly to the substrate. The image of one of these ZnO nanocrystallites is marked in Fig. 6d. The HRTEM and SAED data showed that NPs in the samples **III** and **IV** belong to the hexagonal phase of ZnO.

The UV-Vis-spectrum of the ZnO NPs/PAAm composite hydrogel, recorded relatively to the PAAm hydrogel, had the absorption band related to ZnO with the maximum at $\lambda_{max} = 308$ nm (Fig. S1). This band was shifted to the shorter wavelength region in comparison with the exciton band of the bulk ZnO at ~370 nm, which is characteristic of nanoparticles [20].

The PL spectra of the hydrogels of the ZnO NPs/PAAm composite (sample **III**) and PAAm under excitation at $\lambda_{ex} = 330$ nm are shown in Fig. 7. In both cases, the spectra were broad bands with the emission maxima at $\lambda_{em} = 428$ and 449 nm for the composite and for PAAm, respectively. The presence of ZnO NPs in PAAm matrix caused a shift of the spectrum into the shorter wavelengths region by about 21 nm.

5 Conclusions

The study allowed us to develop simple one-step syntheses of ZnO NPs and ZnO NPs/PAAm hybrid composite. Synthesis procedures do not require special conditions and equipment. The reagents are cheap and available crystalline substances $Zn(CH_3COO)_2{\cdot}2H_2O$ and AAm. The specific features of our synthesis of ZnO NPs by the known reaction of zinc acetate hydrolysis are the use of AAm as the organic base that accepts protons, and the conventional (not absolute) 96% ethanol as the reaction medium. The product of synthesis in ethanol were the crystalline particles of hexagonal ZnO of ~3–5 nm in size, exhibiting yellow photoluminescence with emission maximum at $\lambda_{em} = 590$ nm. Based on the results of chemical analysis, physico-chemical studies and modeling, it was concluded that the surface layer of ZnO nanocrystals consisted of Zn^{2+} and CH_3COO^- ions. The average composition of the NPs was estimated as $\{ZnO\}_{624}\{Zn(CH_3COO)_2\}_{182}$.

The ZnO NPs/PAAm composite was obtained for the first time. The original feature of the synthesis is that the hydrolysis of $Zn(CH_3COO)_2$ was carried out in the aqueous medium, concurrently with the radical polymerization of AAm initiated by $(NH_4)_2S_2O_8$. The product of synthesis was the hydrogel of PAAm with nanocrystals of hexagonal ZnO of ~1–3 nm in size distributed over the hydrogel. The composite hydrogel was colorless, transparent, stable and exhibited photoluminescence with emission maximum at $\lambda_{em} = 431$ nm. The solid ZnO NPs/PAAm composite was precipitated by breaking the hydrogel by the addition of ethanol, in which PAAM is insoluble.

Acknowledgements This work was supported by the Russian Science Foundation (Grant No. 15-13-00080).

Compliance with ethical standards

Conflict of interest The authors declare that they have no competing interests.

References

1. Yu X, Marks TJ, Facchetti A (2016) Metal oxides for optoelectronic applications. Nat Mater 15:383–396. https://doi.org/10.1038/nmat4599

2. Mucur SP, Tumay TA, Birdogan S, San SE, Tekin E (2015) Triangular-shaped zinc oxide nanoparticles enhance the device performances of inverted OLEDs. Nano-Struct Nano-Objects 1:7–14. https://doi.org/10.1016/j.nanoso.2015.01.001
3. Kim DY (2014) Zinc oxide nanostructures for flexible and transparent electronics. Dissertation, Clemson University. http://tigerprints.clemson.edu/all_dissertations/1470. Accessed 16 June 2017
4. Garcia MA, Merino JM, Fernández Pinel E, Quesada A, de la Venta J, Ruiz González ML, Castro GR, Crespo P, Llopis J, González-Calbet JM, Hernando A (2007) Magnetic properties of ZnO nanoparticles. Nano Lett 7:1489–1494. https://doi.org/10.1021/nl070198m
5. Schmidt-Mende L, MacManus-Driscoll JL (2007) ZnO–nanostructures, defects, and devices. Mater Today 10:40–48
6. Krebs FC (2009) Fabrication and processing of polymer solar cells: a review of printing and coating techniques. Solar Energy Mater Solar Cells 93:394–412. https://doi.org/10.1016/j.solmat.2008.10.004
7. Jasieniak J, MacDonald BI, Watkins SE, Mulvaney P (2011) Solution-processed sintered nanocrystal solar cells via layer-by-layer assembly. Nano Lett 11:2856–2864. https://doi.org/10.1021/nl201282v
8. Kolodziejczak-Radzimska A, Jesionowski T (2014) Zinc oxide–from synthesis to application: A review. Materials 7:2833–2881. https://doi.org/10.3390/ma7042833
9. Zhou X, Lee S, Xu Z, Yoon J (2015) Recent progress on the development of chemosensors for gases. Chem Rev 115:7944–8000. https://doi.org/10.1021/cr500567r
10. Tamvakos A, Korir K, Tamvakos D, Calestani D, Cicero G, Pullini D (2016) NO_2 gas sensing mechanism of ZnO thin-film transducers: physical experiment and theoretical correlation study. ACS Sensors 1:406–412. https://doi.org/10.1021/acssensors.6b00051
11. Xiong H-M, Xu Y, Ren Q-G, Xia Y-Y (2008) Stable aqueous ZnO@polymer core-shell nanoparticles with tunable photoluminescence and their application in cell imaging. J Am Chem Soc 130:7522–7523. https://doi.org/10.1021/ja800999u
12. Tang X, Choo ESC, Li L, Ding J, Xue J (2010) Synthesis of ZnO nanoparticles with tunable emission colors and their cell labeling applications. Chem Mater 22:3383–3388. https://doi.org/10.1021/cm903869r
13. Bajpaia SK, Jadauna M, Tiwari S (2016) Synthesis, characterization and antimicrobial applications of zinc oxide nanoparticles loaded gum acacia/poly(SA) hydrogels. Carbohydr Polym 153:60–65. https://doi.org/10.1016/j.carbpol.2016.07.019
14. Javed R, Usman M, Tabassum S, Zia M (2016) Effect of capping agents: structural, optical and biological properties of ZnO nanoparticles. Appl Surf Sci 386:319–326. https://doi.org/10.1016/j.apsusc.2016.06.042
15. Wingett D, Louka P, Anders CB, Zhang J, Punnoose A (2016) A role of ZnO nanoparticles electrostatic properties in cancer cell cytotoxicity. Nanotechnol Sci Application 9:29–45. https://doi.org/10.2147/nsa.s99747
16. Cushing BL, Kolesnichenko VL, O'Connor CJ (2004) Recent advances in the liquid-phase syntheses of inorganic nanoparticles. Chem Rev 104:3893–3946. https://doi.org/10.1021/cr030027b
17. Hosono E, Fujihara S, Kimura T, Imai H (2004) Non-basic solution routes to prepare ZnO nanoparticles. J Sol–Gel Sci Tech 29:71–79
18. Spanhel L, Anderson MA (1991) Semiconductor clusters in sol–gel process: quantized aggregation, gelation, and crystal growth in concentrated ZnO colloids. J Am Chem Soc 113:2826–2833
19. Meulenkamp EA (1998) Synthesis and growth of ZnO nanoparticles. J Phys Chem B 102:5566–5572
20. Wood A, Giersig M, Hilgendorff M, Vilas-Campos A, Liz-Marzan LM, Mulvaney P (2003) Size effects in ZnO: the cluster to quantum dot transition. Aust J Chem 56:1051–1057. https://doi.org/10.1071/ch03120
21. Wong EM, Bonevich JE, Searson PC (1998) Growth kinetics of nanocrystalline ZnO particles from colloidal suspensions. J Phys Chem B 102:7770–7775
22. Wong EM, Hoertz PG, Liang CJ, Shi B-M, Meyer GJ, Searson PC (2001) Influence of organic capping ligands on the growth kinetics of ZnO nanoparticles. Langmuir 17:8362–8367. https://doi.org/10.1021/la010944h
23. Hu Z, Oskam G, Lee Penn R, Pesika N, Searson PC (2003) The influence of anion on the coarsening kinetics of ZnO nanoparticles. J Phys Chem B 107:3124–3130. https://doi.org/10.1021/jp020580h
24. Sun D, Wong M, Sun L, Li Y, Miyatake N, Sue H-J (2007) Purification and stabilization of colloidal ZnO nanoparticles in methanol. J Sol–Gel Sci Technol 43:237–243. https://doi.org/10.1007/s10971-007-1569-z
25. Huang WM, Jiang P, Wei CY, Zhuang DK, Shi J (2008) Low-temperature one-step synthesis of covalently chelated ZnO/dopamine hybrid nanoparticles and there optical properties. J Mater Res 23:1946–1952. https://doi.org/10.1557/jmr.2008.0243
26. Tatarchuk VV, Dobrolubova YuO, Druzhinina IA, Zaikovskii VI, Gevko PN, Maksimovskii EA, Gromilov SA (2016) Facile synthesis of gold nanoparticles in aqueous acrylamide solution. Russ J Inorg Chem 61:535–543. https://doi.org/10.7868/s0044457x16040206
27. Mahdavian A-R, Abdollahi M, Bijanzadeh HR (2004) Kinetic study on radical polymerization. III. Solution polymerization of acrylamide by ^{1}H-NMR. J Appl Polym Sci 93:2007–2013. https://doi.org/10.1002/app.20649
28. Di Benedetto F, Biasco A, Pisignano D, Cingolani R (2005) Patterning polyacrylamide hydrogels by soft lithography. Nanotechnology 16:S165–S170. https://doi.org/10.1088/0957-4484/16/5/006
29. Aftab A, Ismail AR, Khokhar S, Ibupoto ZH (2016) Novel zinc oxide nanoparticles deposited acrylamide composite used for enhancing the performance of water-based drilling fluids at elevated temperature conditions. J Petroleum Sci Eng 146:1142–1157. https://doi.org/10.1016/j.petrol.2016.08.014
30. Powder Diffraction File. PDF-2/Release (2009) International Centre for Diffraction Data. USA. 2009. No 01-076-0704.
31. Murugan R, Mohan S, Bigotto A (1998) FTIR and polarized Raman spectra of acrylamide and polyacrylamide. J Korean Phys Soc 32:505–512
32. Guo Y, Wu P (2008) FTIR spectroscopic study of the acrylamide states in AOT reversed micelles. J Mol Struct 883-884:31–37. https://doi.org/10.1016/j.molstruc.2007.11.009
33. Sun M, Hao W, Wang C, Wang T (2007) A simple and green approach for preparation of ZnO_2 and ZnO under sunlight irradiation. Chem Phys Lett 443:342–346. https://doi.org/10.1016/j.cplett.2007.06.098
34. Bai H, Liu X (2010) Green hydrothermal synthesis and photoluminescence property of ZnO_2 nanoparticles. Mater Lett 64:341–343. https://doi.org/10.1016/j.matlet.2009.11.008
35. AIST: Spectral Database for Organic Compounds, SDBS. http://sdbs.db.aist.go.jp/sdbs/cgi-bin/direct_frame_top.cgi. Accessed 16 June 2017
36. Clegg W, Little IR, Straughan BP, (1986) Monoclinic anhydrous zinc(II) acetate. Acta Cryst C 42:1701–1703
37. He H (2006) A new monoclinic polymorph of anhydrous zinc acetate. Acta Cryst E 62:m3291–m3292. https://doi.org/10.1107/s1600536806046678

38. Kunkely H, Vogler A (1990) Absorption and emission spectrum of $[Zn_40(Acetate)_6]$. J Chem Soc Chem Commun 1204-1205. https://doi.org/10.1039/c39900001204
39. Djurišić AB, Leung YH (2006) Optical properties of ZnO nanostructures. Small 2:944–961. https://doi.org/10.1002/smll.200600134
40. Koksis K, Niedermaier M, Bernardi J, Berger T, Diwald O (2016) Changing interfaces: photoluminescent ZnO nanoparticle powders in different aqueous environments. Surf Sci 652:253–260. https://doi.org/10.1016/j.susc.2016.02.019
41. Gheisi AR, Neygandhi C, Sternig AK, Carrasco E, Marbach H, Thomele D, Diwald O (2014) O_2 adsorption dependent photoluminescence emission from metal oxide nanoparticles. Phys Chem Chem Phys 16:23922–23929. https://doi.org/10.1039/c4cp03080j